ISSN 2070-0482, Mathematical Models and Computer Simulations, 2023, Vol. 15, No. 1, pp. 109–117. © Pleiades Publishing, Ltd., 2023.
Russian Text © The Author(s), 2022, published in Matematicheskoe Modelirovanie, 2022, Vol. 34, No. 7, pp. 49–62.

Numerical Simulation of the Evolution of an Intense Aerodynamic Jet in the Far-Field of Propagation

S. N. Gurbatov[a,*], I. Yu. Demin[a,], A. A. Lisin[a,***], S. A. Karabasov[a,b,****], and A. V. Tyurina[c,*****]**

[a] *Lobachevsky State University, Nizhny Novgorod, Russia*

[b] *Zhukovsky Central Aerohydrodynamic Institute, Zhukovsky, Moscow oblast, 140181 Russia*

[c] *Lomonosov Moscow State University, Moscow, Russia*

**e-mail: gurbatov.sergey@gmail.com*

***e-mail: demin@rf.unn.ru*

****e-mail: lisin.artem.a@gmail.com*

*****e-mail: s.karabasov@qmul.ac.uk*

******e-mail: vanilch22@gmail.com*

Received February 21, 2022; revised February 21, 2022; accepted April 18, 2022

Abstract—The conditions for the outflow of an underexpanded supersonic jet from an experiment conducted at the Laboratory for Turbulent Research in Aerospace and Combustion (LTRAC), Monash University, Australia are considered. The characteristic parameters of linear and nonlinear transport for the LTRAC jet are analyzed using LES solutions from the near and far acoustic fields. In both cases, the fulfillment of the conditions of the linear scenario of sound transfer over distances characteristic of the LTRAC acoustic experiment is shown. To verify the theoretical estimates, numerical solutions of the spherical Burgers equation are also obtained using the initial data from the LES calculation. Solutions are obtained without and in the presence of a term in the Burgers equation corresponding to quadratic nonlinearity. The solutions respond to sound transfer at distances that are orders of magnitude greater than the distance between the acoustic microphone and the jet in the LTRAC experiment.

Keywords: numerical analysis, aeroacoustics, Burgers equation, LTRAC, supersonic jet

DOI: 10.1134/S207004822301009X

1. INTRODUCTION

One of the most important areas of nonlinear acoustics is the study of the acoustic noise of aircraft: their prediction during takeoff and during operation is the most important problem in the development of aviation. Aerodynamic noise is usually emitted in a wide frequency band and is caused, for example, by the unevenness and turbulence of the air flow, when the pressure at the outlet of the aircraft nozzle is not equal to the ambient pressure. This pressure discrepancy is overcome by the jet passing through the regions of expansions and contractions, which are quasi-periodic shock cells interacting with turbulent vortices emanating from the edge of the nozzle. These noise sources are visible in the far-field spectra as multiple peaks near the shock cells. For acoustic waves of sufficiently high amplitude, the steepness of the acoustic wave front can play a significant role in changing the noise spectrum sufficiently far from the source before the linear dissipation mechanism becomes dominant.

Ever since the first Concorde flights [1], the importance of nonlinear effects for the propagation of high-intensity jet noise has been noted. Measurements of jet engine noise at full power have shown that nonlinear distortions of the acoustic spectra have a significant effect on the noise field, and an anomalous enhancement of the high-frequency part of the noise spectrum was found compared to the linear prediction.

However, the effect of nonlinear propagation is not the only possible mechanism for the formation of shock fronts of acoustic waves [2]. In particular, for laboratory-scale jets [3], the effects of nonlinear propagation can be important only in the near field of the jet, while the effect of nonlinearity on the propagation of the far field is insignificant. For example, another mechanism responsible for the formation of shock acoustic waves in the far zone includes the interaction of a shock wave with turbulent shear layers, whose wave structures are linearly transmitted in the far zone [4]. Nonlinear wave propagation competes with the linear effects of atmospheric absorption. The interaction between nonlinear and linear dissipation effects is expressed in terms of the reciprocal acoustic Reynolds number (Goldberg number), which not only strongly depends on the flow conditions such as the pressure-temperature ratio in the nozzle but also on the effective distance to the jet.

To quantify the importance of nonlinear propagation effects on supersonic jet noise, several studies have compared the solution of linear and nonlinear sound propagation models for the same initial conditions. Models in the literature can be divided into two categories. The first category includes theoretical models that use semianalytical solutions of the one-dimensional Burgers equation and the Navier–Stokes equations [5, 6]. These models are computationally efficient but fail to take into account the effects of high Reynolds number turbulence and the distributed nature of supersonic jet noise sources. Compared to them, the second category of models includes fully computational studies that include 3D Navier–Stokes effects, extending the simulation domain to the far field, and combining the Navier–Stokes solution with the Euler solution at a distance from the jet [7]. However, due to the computational costs, these latter models typically use idealized nozzle conditions, such as the jet stream emerging from cylindrical pipe without compression.

Despite the use of high-resolution techniques, such studies usually show limited comparison with the experimental data, especially in the near field of reactive noise. In addition, the range of far-field noise propagation distances considered using such methods is limited to several hundred initial jet diameters, which may not be sufficient for a complete description of nonlinear-linear propagation modes, including the linear dissipation region.

In this paper, we consider modeling the far-field aerodynamic noise generated by a cold supersonic flow of an underexpanded jet in accordance with the conditions of a flow experiment conducted at the Laboratory for Turbulence Research in Aerospace and Combustion (LTRAC) Supersonic Jet Facility at Monash University [8]. The specific jet conditions correspond to the case of the fastest LTRAC jet, when the jet exits the nozzle with a high area ratio at a nozzle pressure ratio of 4.2, producing noticeable shock cells and a Mach disk due to the mismatch between the nozzle exit pressure and ambient pressure. The interaction of shock cells with turbulence in the shear layer leads to intense shock wave noise (BBSAN), which is typical of characteristic peaks in the far-field acoustic spectra for the observation angles from the side. The peaks are primarily related to the regions of interaction between these shock cells and turbulent eddies in the shear layers. To simulate the propagation of the BBASN of an LTRAC jet in the far field, a three-level model was implemented using the domain decomposition approach. In the region of the nonlinear jet flow, the Navier–Stokes equations are solved within the monotonically integrated LES approach, starting from the exit of the nozzle, where the conditions are set from the LTRAC Particle Image Velocimetry (PIV) dataset. The LES results are checked against PIV data. In the second step, the LES solution is combined with the permeable formulation of the Ffowcs Williams–Hawkings (FW-H) method [9, 10] to obtain acoustic near-field noise spectra solutions for several of the most interesting observer angles in terms of BBSAN.

Then the proposed three-level models of acoustic spectra of the near field are used to generate realizations of the initial acoustic noise for the numerical solution of the spherical generalized Burgers equation [2, 11]. The Burgers equation is solved numerically by going into the frequency domain, where the nonlinear partial differential equation for the field is converted into an ordinary differential equation for its Fourier transform, which is approximated by an explicit first-order scheme and solved in the far zone of sound transfer until the distances, at which the effect of linear dissipation is no longer dominant, are reached. To estimate the effect of nonlinearity on the noise spectra in the far zone, the solutions are compared with and without taking into account the nonlinear term in the Burgers equation.

2. NUMERICAL SIMULATION OF THE SOLUTION OF THE EVOLUTIONARY BURGERS EQUATION

We consider the evolutionary Burgers equation describing the propagation of nonlinear spherical waves in viscous media without dispersion [11, 12]

$$\frac{\partial V}{\partial r} + \frac{V}{r} - \frac{\beta}{c^2} V \frac{\partial V}{\partial t} = \frac{b}{2c^3\rho} \frac{\partial^2 V}{\partial t^2}, \tag{1}$$

where $V(r, t)$ is the speed of the acoustic wave, c is the speed of sound in free space, ρ is the density of the medium, b is the kinematic coefficient of viscosity, r is the distance from the wave source, and β is the nonlinear parameter of the medium (for air, approximately 0.5).

Using a change of variables, Eq. (1) can be reduced to the dimensionless Burgers equation for spherical waves

$$\frac{\partial U}{\partial R} - U\frac{\partial U}{\partial \tau} = \varepsilon g(R)\frac{\partial^2 U}{\partial \tau^2}, \tag{2}$$

where the dimensionless quantities are given in the following form:

$$U = \frac{r}{r_0}\frac{V}{V_0},$$
$$\tau = \omega_0 t, \quad x = (r - r_0)/r_{nl}, \quad R_0 = r_0/r_{nl}, \quad R = R_0 \ln((R_0 + x)/R_0), \tag{3}$$
$$r_{nl} = \frac{c^2}{\beta\omega_0 V_0}, \quad r_l = \frac{2c^3\rho}{b\omega_0}, \quad g(R) = \exp(R/R_0).$$

When obtaining Eq. (2) and expressions (3), it was assumed that the initial disturbance of the velocity $V_0(t) = V(t, r = r_0)$ was characterized by some typical amplitude V_0 and frequency ω_0.

Formulas (3) contain two important parameters: the characteristic distance of the formation of discontinuities (shock fronts) in the acoustic wave r_{nl} and the characteristic distance r_l at which the effect of viscous dissipation becomes important. The ratio of these distances determines the reciprocal acoustic Reynolds number $\mathrm{Re}_a^{-1} = \varepsilon = r_{nl}/r_{lin}$ (or the Goldberg number ε). Number R_0 is given as the ratio of the inner radius of the spherical wave source to the characteristic nonlinear distance and determines the range of wave propagation. In addition, the physical meaning of the parameter R_0 is to characterize how far the starting point of acoustic wave emission (effective source) is from the region of interaction of nonlinear waves. It is clearly seen from the dimensionless equation (2) that $\varepsilon g(R)$ plays the role of the effective viscosity coefficient, which, in addition to the ratio of dissipation to nonlinear effects, also contains the wave propagation coefficient [12]. The last factor arises from the fact that, compared to the one-dimensional (plane) propagation of nonlinear waves, the energy of three-dimensional waves is distributed over a spherical surface.

Let us determine the energy spectrum of the acoustic wave

$$E(\omega, R) = V(\omega, R)V^*(\omega, R)$$

through the direct Fourier transform

$$V(\omega, R) = F[V(t, R)] \equiv \frac{1}{2\pi}\int_{-\infty}^{\infty} V(t, R)\exp(-i\omega t)dt. \tag{4}$$

Then the inverse Fourier transform will allow us to determine the wave profile

$$V(t, R) = F^{-1}[V(\omega, R)] \equiv \int_{-\infty}^{\infty} V(\omega, R)\exp(i\omega t)d\omega. \tag{5}$$

The solution of the Burgers equation (2) in the frequency domain can be represented in an iterative form with step ΔR, and F and F^{-1} (denoting the direct and inverse Fourier transform) are determined by formulas (4) and (5)

$$V(\omega, R + \Delta R) = V(\omega, R) + \frac{1}{2}i\omega F[(F^{-1}[V(\omega, R)])^2]\Delta R - \varepsilon\exp\left(R/R_0\right)\omega^2 V(\omega, R)\Delta R. \tag{6}$$

The program for solving the evolutionary Burgers equation for spherical random waves by the pseudospectral method (6) was written in Python.

As the initial condition $V(\omega, R = 0) = V_0(\omega)$ was considered a random process $V_0(\omega) = \xi\sqrt{G_0(\omega)}$, where $\xi = A + iB$ was a random Gaussian process, $\langle A\rangle = \langle B\rangle = 0$, $\langle A^2\rangle = \langle B^2\rangle = 1$, and $G_0(\omega)$ was the initial spectrum, which was chosen in the form [13]

$$G_0(\omega) = \frac{\sigma_0^2}{\omega_*\sqrt{2\pi}}\left(\frac{\omega}{\omega_*}\right)^{2n} \exp(-\omega^2/2\omega_*^2), \quad \sigma_0^2 = 1, \quad \omega_* = 1, \quad n = 1. \tag{7}$$

The maximum of the spectrum is at the frequency $\omega = 2\omega_* = 2$, and the characteristic scale of the manifestation of nonlinearity is equal to $z_{nl} = 1/\sigma_0\omega_1 = 1/\sigma_0\omega_*\sqrt{3} \approx 0.58$. The Reynolds number Re in the experiments was 100. Initial spectrum parameters: $\sigma_0^2 = 1$, $\omega_* = 1$. The averaging was carried out over 1000 realizations, each of which contained 2^{14} readings.

In numerical simulation, two modes of propagation of acoustic noise with the initial spectrum (7) were considered: the first one was the solution of the original nonlinear problem (6) and the second one was the solution of the linear problem, which corresponded to the artificial removal of the quadratic velocity term from the right side of Eq. (6). This was done to evaluate the effect of nonlinearity on acoustic noise propagation. Figure 1 shows a comparison of the evolution of acoustic noise for the linear (Fig. 1a) and nonlinear (Fig. 1b) propagation modes at different distances from the source: the given distance (x/R_0).

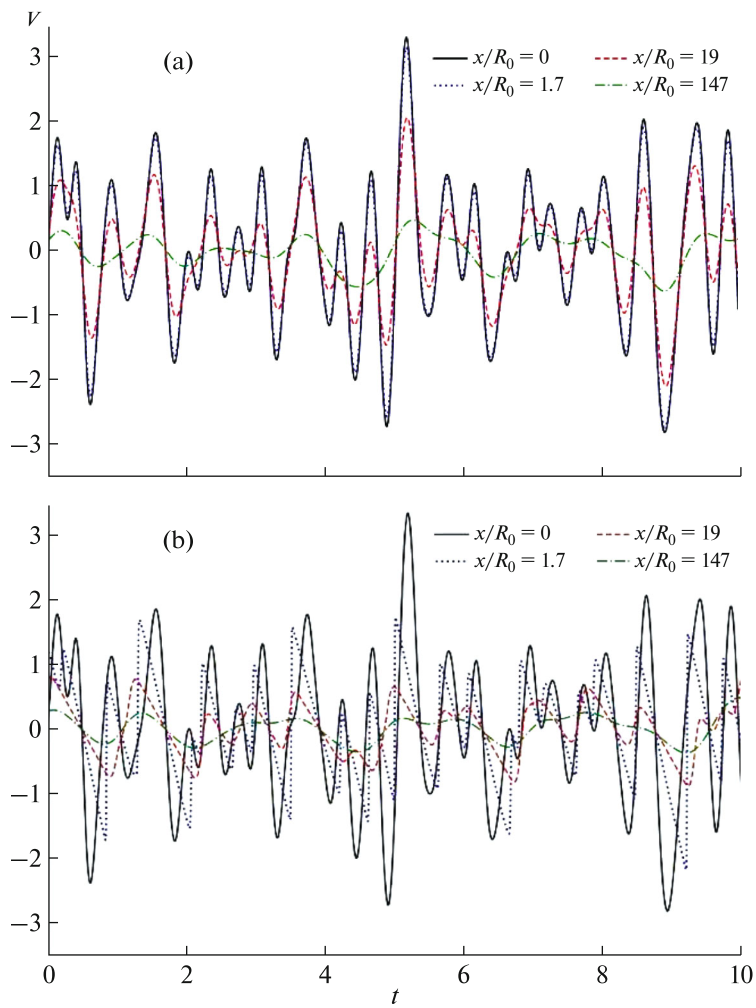

Fig. 1. (a) Evolution of a spherical acoustic wave for the Reynolds number Re = 100 and various distances from the source x/R_0 for the solution of a linear model; (b) Evolution of a spherical acoustic wave for the Reynolds number Re = 100 and various distances from the source x/R_0 for the solution of a nonlinear model.

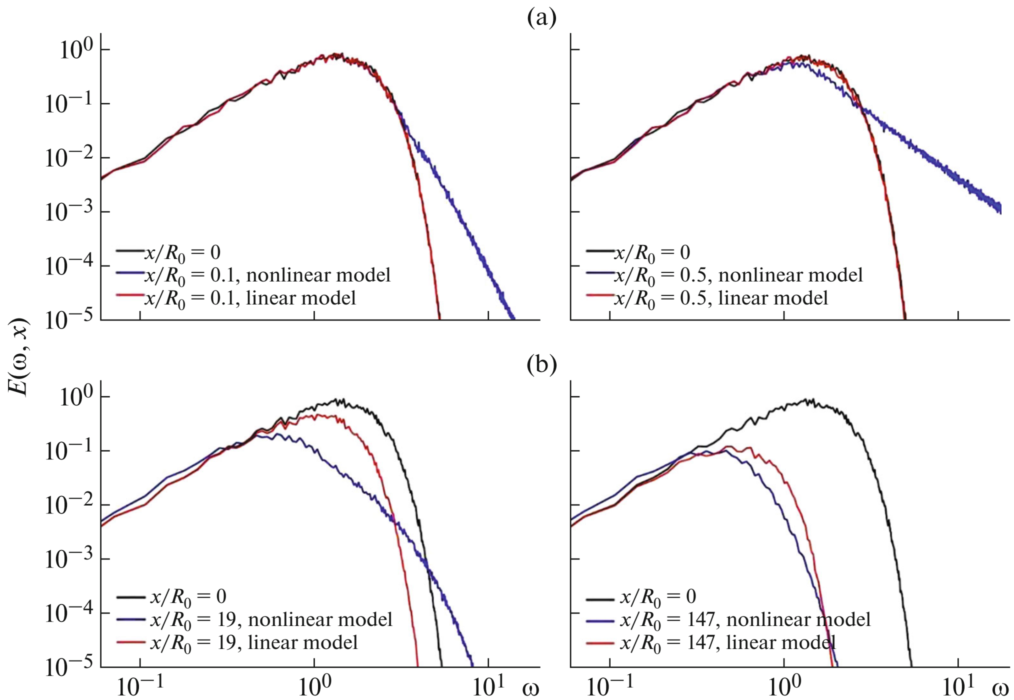

Fig. 2. (a) Evolution of energy spectra for the Reynolds number Re = 100 for the solution of linear and nonlinear models at distances before the formation of a discontinuity of $x/R_0 = 0.1$ (left) and $x/R_0 = 0.5$ (right); (b) Evolution of energy spectra for the Reynolds number Re = 100 for the solution of linear and nonlinear models at the stage of developed discontinuities of $x/R_0 = 19$ (left) and $x/R_0 = 147$ (right).

From the profiles of the spherical random wave given above, it is clearly seen that at $x/R_0 = 1.7$ for the nonlinear model, sawtooth wave fronts appear in the solution, which subsequently leads at the stage of developed discontinuities to the merging of nonlinear fronts—there is a rapid decay of the amplitudes of the nonlinear wave profiles compared to the regime of linear propagation of spherical random waves.

Figure 2 shows the evolution of the energy spectra for the linear and nonlinear model of the numerical solution according to scheme (6) in the frequency domain for the distances up to the formation of discontinuities (Fig. 2a) and at the stage of developed ruptures (Fig. 2b) in a spherical random wave.

From Fig. 2a at short distances from the source (before the formation of discontinuities in the profiles of spherical random waves at $r - r_0 < r_{nl}$), it can be seen that, except for the high-frequency region, the nonlinear model does not differ from the linear propagation model, apart from the high frequencies—the spectra are barely affected by nonlinearity. At long distances (Fig. 2b), which correspond to the stage of interaction of the developed discontinuities ($r_{nl} < r - r_0 < r_l$), the nonlinear interaction of the waves leads to faster dissipation, a decrease in energy and a shift of the spectrum maximum to the low-frequency region, which differs from the linear mode of the evolution of random waves ($x/R_0 = 19$). There is also a difference between the linear and nonlinear solutions for the energy spectra in the high-frequency part until the dissipation mechanism becomes definitive for most of the noise spectrum ($x/R_0 = 147$).

3. LTRAC SUPERSONIC JET: FAR FIELD SIMULATION

The supersonic underexpanded jet stream considered as the initial conditions corresponds to the conditions of the experiment carried out at the LTRAC [18]. In the LTRAC experiment, compressed air is supplied to the plenum chamber at a temperature of approximately $T_k = 288$ K. The plenum was connected to the mixing chamber under normal atmospheric conditions, where the velocity measurements of the flow were taken by laser diagnostics with a high spatial resolution (PIV). Compressed air exits from an axisymmetric nozzle $D_j = 15$ mm with a 5-mm-thick edge. The fully expanded flow conditions are $M_{\text{fe}} = 1.59$ NPR = 4.2, $D_{\text{ef}} = 16.73$ mm, and Re = 1.06×10^6. The nozzle has an inlet to outlet area ratio of 93.44 with a short converging section so that the outlet flow is sonic at a velocity of $U_j = 310$ m/s. The converging

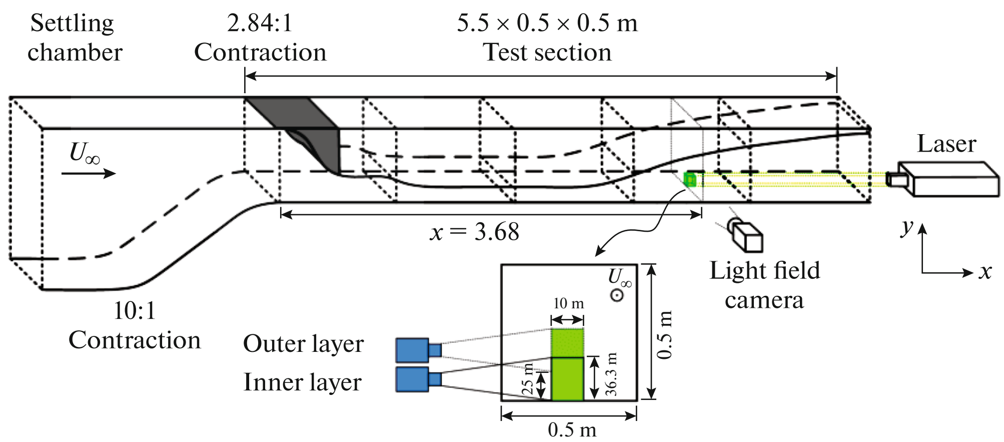

Fig. 3. Scheme of the LTRAC experiment.

section consists of a profiled wall with a curvature radius of 67.15 mm and a short parallel section at the outlet (Fig. 3).

To simulate the flow of the LTRAC jet, the Cabaret scheme is used in the framework of the large eddy method (MILES). Cabaret's properties include low dispersion and dissipative error. The use of a space-time spaced compact computational template and an explicit asynchronous time step in Cabaret provides good accuracy on inhomogeneous grids. Inhomogeneous grids are built semi-automatically using the OpenFOAM snappyHexMesh (sHM) utility [14–16]. The Cabaret calculation results for the average longitudinal flow velocity are compared with the experiment on two computational grids in Fig. 4.

The LES grid of the LTRAC jet contains 41 million cells and starts from the nozzle exit. The flow conditions at the nozzle outlet are set using the flow and radial mean flow velocity from the PIV data by superimposing the nozzle outlet sonic conditions and assuming the same stagnation pressure as in the upstream chamber. The grid is locally thickened near the nozzle edge, and the resolution of the grid in the longitudinal, radial, and azimuthal directions is $\Delta x/D_j = 0.02$, $\Delta r/D_j = 0.011$, and $r\Delta\theta/D_j = 0.02$.

For higher frequencies, the current LES solution is not sufficiently resolved. However, the main peak of the BBSAN spectra around 0.4–0.5 is clearly captured by the LES solution, especially at an observation angle of 120°. The peak of the BBSAN hump is 12–15 dB higher than the frequency amplitude of about 0.2–0.3, which corresponds to the peak jet mixing noise for the same side viewing angles and is shown in Fig. 2.

The two initial conditions for the propagation of a spherical wave are considered: the acoustic velocity spectra obtained from the LES-FW-H solution at an observer angle of 90° and 120°. First, the LES solution in the acoustic near field at $0 < x/DJ < 3$ and $r/DJ = 3$ is used to estimate the characteristic velocity fluctuation at the initial radius of a source that is close to the intense BBSAN source but does not have a noticeable distortion by the hydrodynamic field. For the second set of initial conditions, the solution of the pressure spectra obtained by the FW-H method at $R/D_j = 20$ and an observation angle of 90° relative to the jet stream, is converted to the characteristic velocity oscillation under the assumption of a linear relationship between the pressure and velocity oscillations in the acoustic wave $u' \sim p'/(\rho \cdot c)$. For both of these datasets, the corresponding sound wave propagation frequency can be estimated from the BBSAN peak frequency, which for the LTRAC jet is 13.12 kHz.

In general, this completely determines the parameters for the numerical analysis of the evolutionary Burgers equation (2) and (3), whose solution is described by a pseudospectral scheme in the frequency domain (6), and which are summarized in Table 1.

Table 1. Input parameters of the initial jet for the numerical analysis of the evolutionary Burgers equation in the far propagation zone

Initial parameters	r_l	r_{nl}	ε	R_0
LES for $R/D_j = 3$	38841.34	14.6	0.000375802	0.0031
LES and FW-H for $R/D_j = 20$	38841.34	7470	0.1923	0.00004

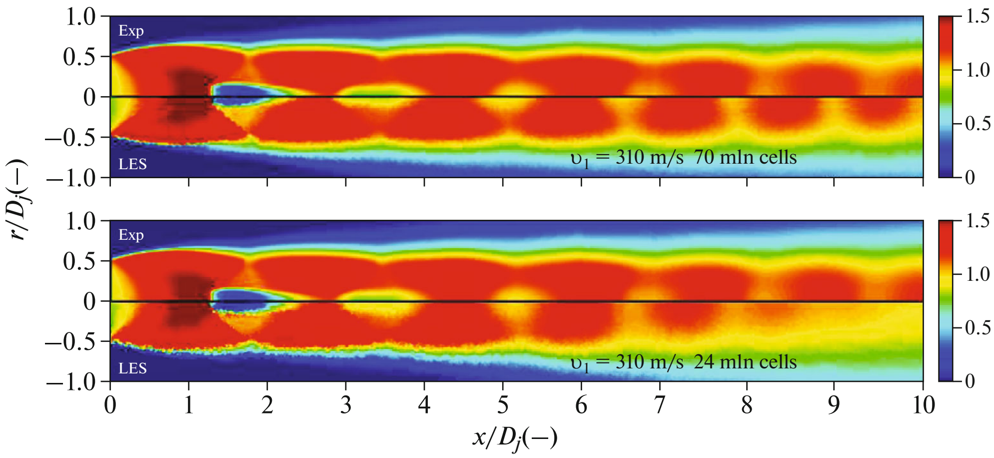

Fig. 4. Visualization of the comparison of the results of the experiment and the model (on a fine grid of 70 million cells and a coarse grid of 24 million cells).

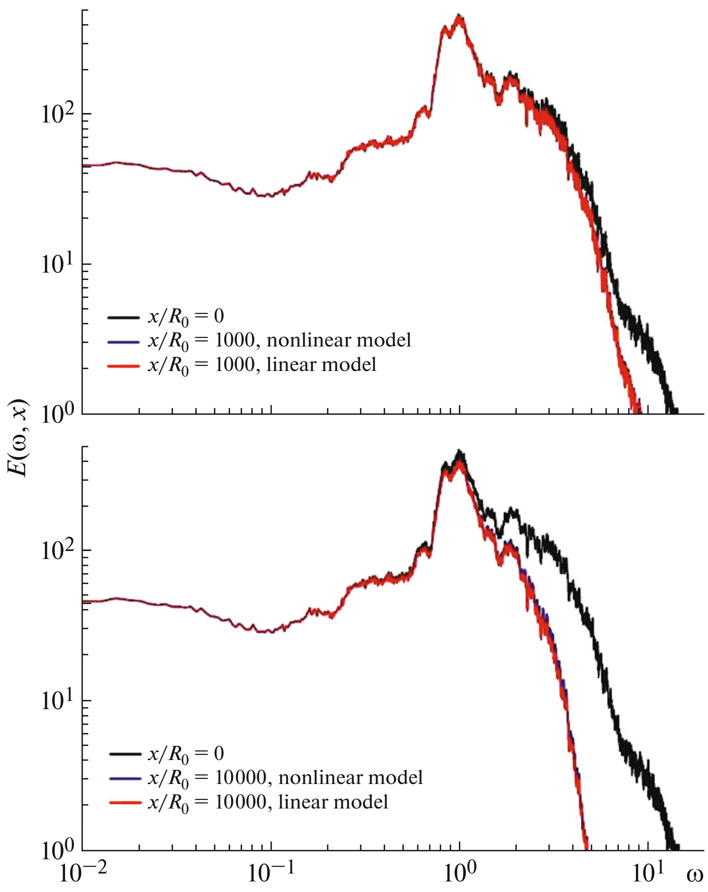

Fig. 5. Energy spectrum of the LTRAC supersonic jet in the far field at distances of about 20000 D_j (a) and 200000 D_j (b). The initial spectrum was determined from the LES and FW-H solution method for distances of 20 D_j from the nozzle. A comparison is made between the linear and nonlinear models for modeling the Burgers equation.

It can be noted that both sets of data given in Table 1 qualitatively correspond to the same mode of propagation of acoustic waves $R^0 \ll r_{nl} \ll r_l$. This means that the source of spherical random waves is located far from the region of the formation of nonlinear waves and where the formation of shock fronts and the effects of viscous dissipation take place.

At the next stage, the acoustic spectrum at an observation angle of 90° with $R/D_j = 20$ is scaled appropriately and then used as the initial condition to replace the analytical Gaussian energy spectrum (7). After determining the initial spectrum, the problem of spherical wave propagation (2)–(6) is solved for 1000 realizations. The obtained spectral solutions, averaged over the ensemble at two distances from the source, are shown in the figure for both linear and nonlinear sound propagation models. The initial spectrum is also shown in Fig. 5.

It can be seen that the nonlinear solution of the Burgers equation does not qualitatively differ from the linear one, while the fronts of acoustic waves do not show significant steepening. This explains why, for the considered LTRAC jet, nonlinearity does not play a role in the formation of noise spectra in the far field.

4. CONCLUSIONS

In order to answer the question on whether nonlinear acoustic propagation effects can be important for the studied LTRAC jet over long propagation distances, a generalized Burgers model is considered that describes the propagation of spherical waves. To numerically solve the Burgers equation, a pseudospectral solution method in the frequency domain is used to obtain the energy spectra of a spherical acoustic wave at various distances from the source. It is shown that, in accordance with the theory, depending on how the distance of the wave from the source is related to the nonlinear and linear-viscous scales of the problem, the numerical solution reveals either the initial linear regime, the nonlinear regime of wave interaction, or the linear regime of viscous dissipation. Furthermore, using the LTRAC jet LES solution as the input to the Burgers equation, it has been shown that even at wave distances up to 200000 nozzle diameters from the nozzle exit (a distance of 3 km), sound propagation is completely determined by linear effects, where the effects of the nonlinear interactions of noise waves are negligible. Therefore, the case of the considered LTRAC jet falls into the category of small-scale supersonic jets, where the nonlinear wave effects that are important for the jet in the near field become insignificant for acoustic wave propagation in the far field.

FUNDING

This study was supported by the Russian Science Foundation, project no. 19-12-00256.

REFERENCES

1. C. L. Morfey and G. P. Howell, "Nonlinear propagation of aircraft noise in the atmosphere," AIAA J. **19** (8), 986–992 (1981).
https://doi.org/10.2514/3.51026
2. S. N. Gurbatov and O. V. Rudenko, "Statistical phenomena," in *Nonlinear Acoustics*, Ed. by M. F. Hamilton and D. T. Blackstock (Academic, San Diego, CA, 1998), Ch. 13, pp. 377–398.
3. W. Baars, C. Tinney, M. Wochner, and M. Hamilton, "On cumulative nonlinear acoustic waveform distortions from high-speed jets," J. Fluid Mech. **749**, 331–366 (2014).
https://doi.org/10.1017/jfm.2014.228
4. M. F. Hamilton, "Effective Gol'dberg numbers for diverging waves," J. Acoust. Soc. Am. **140** (6), 4419–4426 (2016).
https://doi.org/10.1121/1.4968787
5. K. L. Gee, V. W. Sparrow, M. M. James, J. M. Downing, C.M. Hobbs, T.B. Gabrielson, and A.A. Atchley, "The role of nonlinear effects in the propagation of noise from high-power jet aircraft," J. Acoust. Soc. Am. **123** (6), 4082–4093 (2008).
https://doi.org/10.1121/1.2903871
6. P. Pineau and C. Bogey, "Numerical investigation of wave steepening and shock coalescence near a cold Mach 3 jet," J. Acoust. Soc. Am. **149** (1), 357–370 (2021).
https://doi.org/10.1121/10.0003343
7. D. Edgington-Mitchell, K. Oberleithner, D. R. Honnery, and J. Soria, "Coherent structure and sound production in the helical mode of a screeching axisymmetric jet," J. Fluid Mech. **748**, 822–847 (2014).
https://doi.org/10.1017/jfm.2014.173
8. J. E. Ffowcs Williams, and D. L. Hawkings, "Sound generation by turbulence and surfaces in arbitrary motion," Philos. Trans. R. Soc. A Math., Phys. Eng. Sci. **264** (1151), 321–342 (1969).
https://doi.org/10.1098/rsta.1969.0031

9. M. L. Shur, P. R. Spalart, and M. Kh. Strelets, “Noise prediction for increasingly complex jets. Part I: Methods and tests,” Int. J. Aeroacoust. **4** (3), 213–245 (2005). “Noise prediction for increasingly complex jets. Part II: Applications,” Int. J. Aeroacoust. **4** (3), 247–266 (2005).
https://doi.org/10.1260/1475472054771385
https://doi.org/10.1260/1475472054771376
10. S. N. Gurbatov, O. V. Rudenko, and A. I. Saichev, *Waves and Structures in Nonlinear Nondispersive Media*: *General Theory and Applications to Nonlinear Acoustics* (Fizmatlit, Moscow, 2008; Springer, Berlin, 2011).
https://doi.org/10.1007/978-3-642-23617-4
11. S. N. Gurbatov, I. Yu. Demin, Val. V. Cherepennikov, and B. O. Enflo, “Behavior of intense acoustic noise at large distances,” Acoust. Phys. **53** (1), 48–63 (2007).
https://doi.org/10.1134/S106377100701006X
12. S. N. Gurbatov, O. V. Rudenko, and A. V. Tyurina, “Singularities and spectral asymptotics of a random nonlinear wave in a nondispersive system,” Wave Motion **95**, 102519 (2020).
https://doi.org/10.1016/j.wavemoti.2020.102519
13. V. A. Semiletov and S. A. Karabasov, “CABARET scheme with conservation-flux asynchronous time-stepping for nonlinear aeroacoustics problems,” J. Comput. Phys. **253**, 157–165 (2013).
https://doi.org/10.1016/j.jcp.2013.07.008
14. A. P. Markesteijn and S. A. Karabasov, “CABARET solutions on graphics processing units for NASA jets: Grid sensitivity and unsteady inflow condition effect,” C. R. Méc. **346** (10), 948–963 (2018).
https://doi.org/10.1016/j.crme.2018.07.004
15. A. P. Markesteijn and S. A. Karabasov, “Simulations of co-axial jet flows on graphics processing units: The flow and noise analysis,” Philos. Trans. R. Soc. A Math. Phys. Eng. Sci. **377** (2159), 20190083 (2019).
https://doi.org/10.1098/rsta.2019.0083